Batteries & Supercaps

Research Article
doi.org/10.1002/batt.202100415

Chemistry Europe
European Chemical Societies Publishing

www.batteries-supercaps.org

In Situ Hydrogen Evolution Monitoring During the Electrochemical Formation and Cycling of Pressed-Plate Carbonyl Iron Electrodes in Alkaline Electrolyte

Henning Weinrich,*[a] Jan Pleie,[a] Bernhard Schmid,[a] Hermann Tempel,[a] Hans Kungl,[a] and Rüdiger-A. Eichel[a, b]

The hydrogen evolution reaction (HER) on iron is a parasitic side reaction for the reduction of iron (hydr)oxide in alkaline electrolyte, which lowers the Coulombic efficiency of iron-based batteries. Tackling this issue, here we investigate the HER on iron electrodes by in situ gas chromatography, allowing for a quantitative correlation of the applied electrode potential and the resulting hydrogen evolution. As a result, it is shown that the HER follows a distinctive profile corresponding to the electrode potential and changes depending on the state of the iron electrode formation. Moreover, it is shown that the charging efficiency of the iron electrode can be increased by an alteration of the charging procedure, i.e., a more negative cut-off potential for the discharge and a potential limitation for the recharge. In this study, a charging efficiency of 96.7% is achieved, using an optimized charging procedure for a formed carbonyl iron electrode containing 8.5 wt.% of Bi_2S_3.

Introduction

Aiming at a CO_2 neutral society, various ideas have to be implemented realizing grid stability and continuous material supply despite fluctuating feed-in by renewable energy sources and the intended fade-out of fossil resources.[1,2] Power-to-X technologies, with X representing various substance classes such as gases, chemicals or liquids provide a great opportunity to achieve this goal. In fact, Power-to-X technologies allow for the storage of renewable electricity for time-delayed consumption or provide base chemicals for a circular carbon economy.[3–5] Furthermore, with X standing for metals, Power-to-X as a keyword also covers the field of metal-air battery research, while Power-to-Metal-to-Power describes the cycling procedure, i.e., charge and discharge, of a secondary cell.

Among the various types of metal-air batteries, iron-air batteries stand out, given the vast abundance of iron, a decent theoretical energy density of 9677 Wh/L_{Fe} (or 1228 Wh/kg_{Fe}, excl. oxygen uptake), a potentially low price[6] and a preeminent environmental friendliness.[7–10] Moreover, iron is less prone to form dendrites upon electrochemical cycling in alkaline media than zinc,[8,11] with all of the aforementioned aspects ever-sparking research and commercial interest since the times of Thomas Alva Edison.[12,13] However, after a well advanced attempt of commercialization for automotive purposes in the 1970's,[14,15] iron-air batteries almost disappeared due to several issues such as spontaneous hydrogen evolution due to self-discharge (corrosion of iron) and water splitting during the recharge (parasitic side reaction) as well as unsatisfactory air electrode performance.[8,14] Renewed interest in iron-air batteries was generated by research activities in the United States[16,17] and the United Kingdom[18,19] starting from 2012 and 2015, respectively. Since then, most researchers particularly focused on the development of various iron electrodes,[20–28] which are unique for iron-air batteries, while air electrodes are being investigated in a broader context of alkaline metal-air batteries in general.[29–31]

En route to highly efficient rechargeable iron electrodes, several researchers have achieved promising results in terms of charging efficiency,[32] which can be as high as 97% at a long-term stable discharge capacity of up to 200 mAh/g_{Fe} for 3500 consecutive charge/discharge cycles.[33] Moreover, temporarily higher discharge capacities of 400 mAh/g_{Fe}[34] and 550 mAh/g_{Fe}[28] have been reported, too, but for inferior charging efficiencies, e.g., 80% and 57%. Two main reasons for the difference in performance of various electrodes lie in i) the choice of active material, which may either consist of iron oxide nanoparticles or macroscopic iron particles,[7] and ii) the applied cycling procedure, which would either seek to exploit the full capacity of both possible oxidation reactions[21,28] (Fe(0)→Fe(II)→Fe(III)) or avoids deep discharge by a discharge potential limitation to the first oxidation reaction (Fe(0)→Fe(II)).[9,23] In case of macroscopic iron particles such as carbonyl iron (particle size: 3–10 μm) the electrochemical oxidation during the discharge is typically limited to an iron electrode potential

[a] Dr. H. Weinrich, J. Pleie, B. Schmid, Dr. H. Tempel, Dr. H. Kungl, Prof. Dr. R.-A. Eichel
Institute of Energy and Climate Research – Fundamental Electrochemistry (IEK-9)
Forschungszentrum Jülich GmbH
Wilhelm-Johnen Str., 52428 Jülich, Germany
E-mail: h.weinich@fz-juelich.de
[b] Prof. Dr. R.-A. Eichel
Institute of Physical Chemistry
RWTH Aachen
Landoltweg 2, 52074 Aachen, Germany

Supporting information for this article is available on the WWW under https://doi.org/10.1002/batt.202100415

Research Article
doi.org/10.1002/batt.202100415
Chemistry Europe
European Chemical Societies Publishing

of −0.75 V vs. Hg/HgO, which marks the transition from one oxidation reaction to the other and allows for extended electrochemical cycling of the iron electrode.[17,22,23] However, given the initially limited surface area of macroscopic iron particles, in the beginning, the discharge capacity of carbonyl iron electrodes is limited as well, but increases due to formation upon repeated oxidation and reduction.[17,23,35,36] During and at the end of this process, the maximum discharge capacity of carbonyl iron electrodes is limited by the applied charge capacity, since the iron electrode reduction during the recharge provides the active surface area for the subsequent discharge by the reduction of accumulated iron (hydr)oxide.[22] Excess and diverted charge during the reduction is allegedly consumed by hydrogen evolution as a competing parasitic side reaction,[37–39] since iron is also a suitable non-noble transition metal catalyst for water splitting.[40] Accordingly, the hydrogen evolution reaction (HER), which may be suppressed by electrode-[20,38,41] and electrolyte additives,[37,39,42] is of fundamental importance for the efficiency of the iron electrode reduction. However, despite its importance, the HER has rarely been investigated directly, i.e., the resulting amount of evolved hydrogen has rarely been determined in correspondence with the applied electrode potential.[43]

Therefore, the purpose of the present investigation is to monitor the HER during the formation and electrochemical cycling in the steady-state of pressed-plate carbonyl iron electrodes, which are known to provide decent discharge capacities of up to $Q_{dis} = 225$ mAh/g_{Fe} for a charging capacity of $Q_{chr} = 300$ mAh/g_{Fe}[22] and excellent stability for an extended number of at least 400 charge/discharge cycles.[36] With this, the present study provides useful insights into the electrochemical processes that prevent iron electrodes from even higher charging efficiencies and clearly links the HER-intensity to the applied electrode potential depending on the state of the iron electrode formation.

Results and Discussion

Formation behavior

Figure 1 shows the progression of the electrochemical formation for a custom-made, pressed-plate carbonyl iron electrode containing 8.5 wt.% of Bi_2S_3. For the present investigation, −0.75 V vs. Hg/HgO was used as a discharge potential limit in order to prevent deep discharge of the iron electrode due to the oxidation of $Fe(OH)_2$ to any Fe(III)-containing species such as $Fe(OH)_3$, FeOOH or Fe_3O_4.[17,44] Given the repeated oxidation and reduction in 6 M KOH electrolyte, the discharge capacity (Q_{dis}) of the investigated electrode slowly increases over the

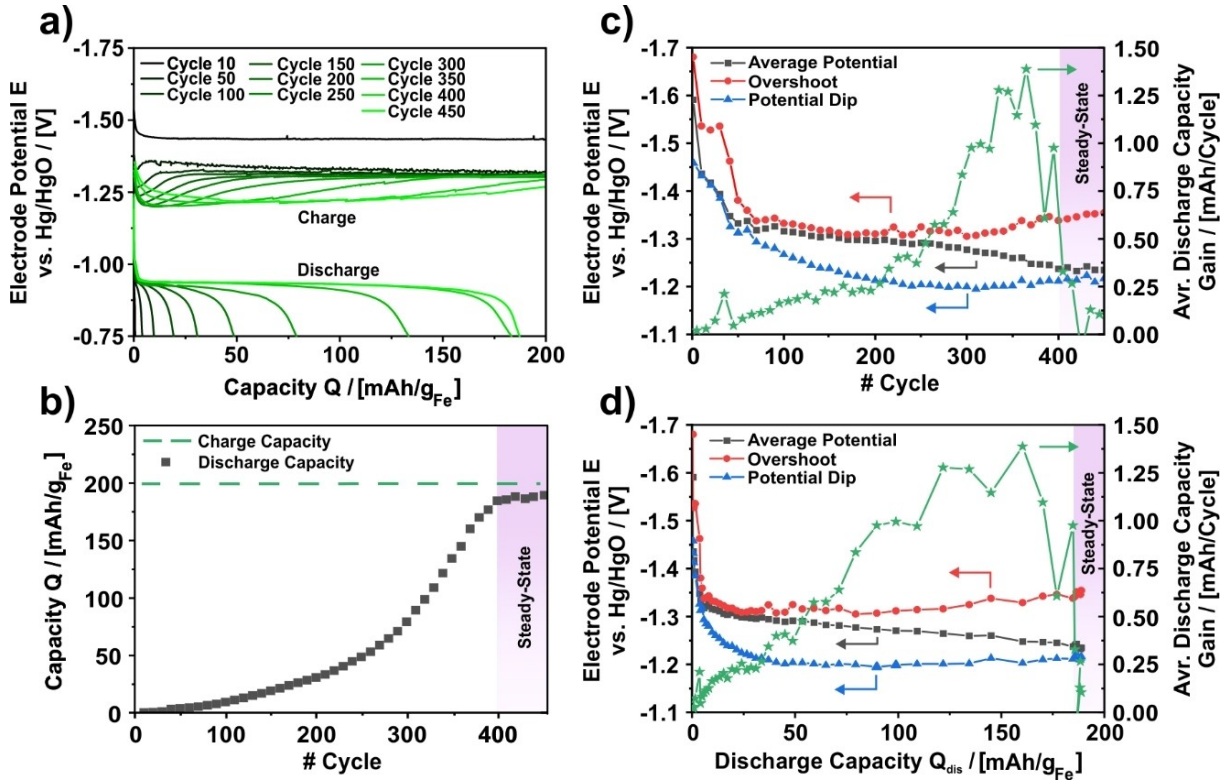

Figure 1. Formation behavior of a pressed-plate carbonyl iron electrode (Formation conditions: $I_{chr} = -200$ mA, $Q_{chr} = 200$mAh/g_{Fe}, $I_{dis} = 20$ mA, 6 M KOH, ambient temperature, for an allocation of overshoot, potential dip and potential plateau see also Figure S2). a) Selected charge/discharge potential profiles. b) Corresponding progression of the discharge capacity due to repeated oxidation and reduction. c) Course of the average potential, overshoot potential and dip potential for individual reduction cycles along with the corresponding cycle number. d) Course of the average potential, overshoot potential and dip potential for individual reduction cycles along with the corresponding discharge capacity. Red shaded areas indicate the end of formation (= steady-state of the iron electrode discharge capacity).

course of 400 formation cycles (Figure 1a). The increase in discharge capacity along with the electrochemical cycling is a result of a continuously increasing iron electrode surface area due to the coarsening of the individual carbonyl iron particles[17,22,23,35] and an increasing material utilization due to an increasing accessibility of the inner electrode volume.[36] Furthermore, the extended number of formation cycles is a result for the extended thickness of the investigated iron electrodes as compared to other results.[17,36,45] During the electrochemical cycling, the iron electrode oxidation, which would occur during the discharge of an iron-air battery, relies on the conversion of Fe to $Fe(OH)_2$, according to the following reaction.[20–28] (All electrode potentials in this paper are reported with respect to the Hg/HgO reference potential (+0.098 V vs. standard hydrogen electrode, SHE) unless stated otherwise):

$$Fe + 2\ OH^- \rightarrow Fe(OH)_2 + 2\ e^- \quad E^0 = -0.88\ V\ vs.\ SHE \qquad (1)$$

In the applied experimental set-up (see Figure S1), the reaction according to Equation (1) occurs at a fairly stable electrode potential in a range from −1.0 V to −0.90 V with a rather sudden jump to more positive potentials once the available iron is mostly depleted due to the successive coverage of the active surface by the corresponding oxidation product, $Fe(OH)_2$.[17,23] Upon recharge, the accumulated $Fe(OH)_2$ is reduced back to Fe, resulting in a distinctive but potential-wise changeable course of the potential profile depending on the state of the iron electrode formation (Figure 1a). During the reduction, the investigated type of electrode typically shows a potential overshoot in the beginning, a potential dip in the middle and a stable potential plateau at the end of the charging step (see Figure S2).[22,23] However, the stable potential plateau will only be observed in case the applied charge capacity (Q_{chr}) is considerably higher than the currently available discharge capacity. (For a detailed description of the corresponding electrode potential see Figures 1c–d). For the present investigation, a constant charge capacity of $Q_{chr} = 200\ mAh/g_{Fe}$ was applied to the investigated iron electrode in every charge step, eventually leading to a discharge capacity (Q_{dis}) of $Q_{dis} = 188.2\ mAh/g_{Fe}$ in the steady-state of the discharge capacity (Figure 1b). The latter corresponds to a charging efficiency (CE) of $CE(Q_{chr}) = 94.1\%$, which is a reasonable result as compared to previous studies, which report up to $CE(Q_{chr}) = 96\%$ for a comparable composition but a lower electrode thickness.[16] Moreover, once the discharge capacity of the electrode reached the steady-state after 400 formation cycles, the cycling procedure was maintained for another 50 cycles prior to subsequent experiments, demonstrating the stability of the electrode for the applied charge capacity, which corresponds to 20.7% of the theoretic capacity of iron (964 mAh/g_{Fe}).

Making it more obvious that the investigated electrode reached a steady-state for the discharge capacity, Figures 1c–d display the progression of the discharge capacity in terms of the average discharge capacity gain per cycle depending on the number of formation cycles (Figure 1c) and the available discharge capacity (Figure 1d). In the individual plots it can be seen that the average discharge capacity gain per cycle almost continuously increases until the electrode attains a capacity of about 160 mAh/g_{Fe} after 360 cycles. Afterwards, the average discharge capacity gain per cycle starts to decrease and drops to 0.25 mAh/cycle and below, indicating the steady-state.

Along with the average discharge capacity gain per cycle, Figures 1c–d show the evolution for the potential of distinctive charge potential profile features, i.e., overshoot and dip potential, as well as the average electrode potential calculated as the mean value of each individual charging cycles based on charging time. From the coinciding display of the electrode potentials and the average discharge capacity gain per cycle, it can be seen that the average electrode potential during the recharge is constantly increasing from about −1.6 V to −1.23 V and remains fairly constant, once the steady-state of the discharge capacity has been attained. At the same time it can be seen that the overshoot potential increases from about −1.7 V to a fairly steady maximum of −1.30 V in the middle of the formation period, but starts to increase again once the electrode lead to a discharge capacity > 100 mAh/g_{Fe} after 325 cycles. The present observation suggests a twofold origin of the potential overshoot for the investigated electrode: i) In the beginning of the formation, the overshoot peak appears to result from a high charging overpotential that might stem from a limited overall surface area as the coarsening of the carbonyl iron particles during the formation did not reach an advanced state yet, leading to a comparatively high true charge current density. ii) On the other hand, once the formation yielded a larger available surface area at the end of the formation period, the amount of discharge product that accumulated on the iron electrode is also larger, potentially leading to a higher resistance of the passivating layer and, with this, to a higher charging potential as compared to the beginning of the formation.

Furthermore, looking at the progression of the dip potential, in Figures 1c–d it can be seen that the corresponding values start to increase from about −1.45 V and reach a maximum at about −1.20 V. The dip corresponds to the predominant reduction of $Fe(OH)_2$ back to Fe with a smooth transition to the hydrogen evolution reaction (HER), as the amount of available $Fe(OH)_2$ decreases.[22,23] With this, the dip potential follows the subordinate trend of a decreasing average charging potential as the available active surface area of the iron electrode increases along with the formation. However, at the end of the formation period, the dip potential is influenced by the reincrease of the overshoot potential since the overshoot peak overlaps with the dip potential region and leads to an increasing potential value for the dip beyond cycle 310.

HER monitoring

Hydrogen evolution due to water splitting is a competing parasitic side reaction for the iron electrode reduction, which lowers the charging efficiency for the electrochemical cycling of iron electrodes.[37–39] Monitoring the HER during the recharge along with the electrochemical formation and cycling of the investigated electrode, Figure 2 provides a selected set of charge potential profiles (Figure 2a) together with the corresponding course of the HER, introduced by the Faradaic

Research Article
doi.org/10.1002/batt.202100415
Chemistry Europe
European Chemical Societies Publishing

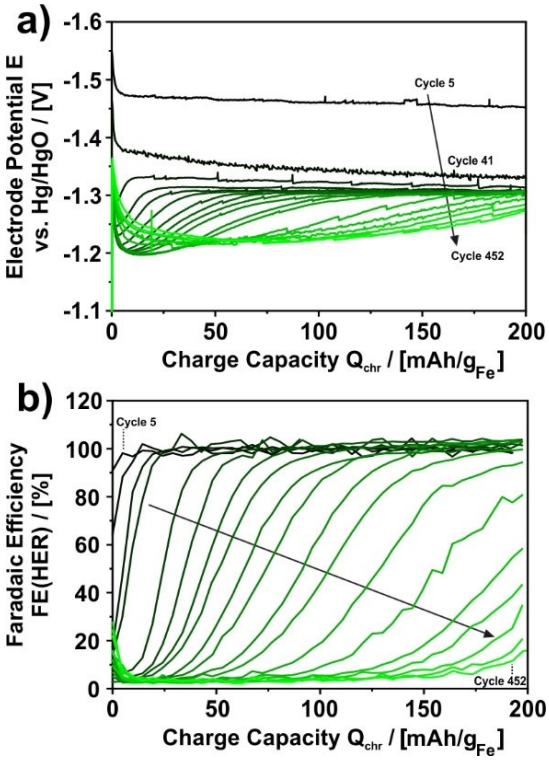

Figure 2. Course of the hydrogen evolution reaction (HER) during the formation and continuous electrochemical cycling of a pressed-plate carbonyl iron electrode in 6 M KOH at ambient temperature. a) Electrode potential during the iron electrode reduction. b) Corresponding Faradaic efficiency (FE) of the HER as determined by in situ gas chromatography. (For an exemplary analysis of the raw data see Figure S2.)

efficiency for the HER, FE(HER), as shown in Figure 2b. FE(HER) was calculated based on in situ gas chromatography (GC) measurements using Equation (2) that is typically applied for gas evolution measurements (for a complete list of denotations see the Supporting Information):[46]

$$FE(HER) = \frac{z_{H2} \cdot F \cdot \frac{p}{RT} \cdot \dot{V}_{out} \cdot c_{H2}}{\dot{Q}} \cdot 100\% \quad (2)$$

In Figure 2b it can be seen that FE(HER) evolves continuously along with the electrochemical formation. Moreover, it is clear that the course of the individual HER curves corresponds to the course of the respective charge potential profiles shown in Figure 2a. As a general observation it can be said that the more positive the iron electrode potential is, the lower the corresponding HER-intensity will be. The latter can particularly be observed for a comparison of cycle 5 and cycle 452 (see also Figure S3). In cycle 5, FE(HER) almost immediately reaches FE(HER) = 100 %, while the average (Avr.) FE(HER) is as high as 98.7 %, since the iron electrode potential is constantly more negative than −1.45 V, i.e., well below the standard electrode potential of the HER [Eq. (3)]:[20–28]

$$2\ H_2O + 2\ e^- \rightarrow H_2 + 2\ OH^- \quad E^0 = -0.83\ V\ vs.\ SHE \quad (3)$$

On the other hand, for cycle 452, FE(HER) is always lower than FE(HER) = 30 % and mostly lower than 6 %, Avr. FE(HER) = 5.9 %, with the beginning and the end of the recharge step being an exception. Thus, the electrical charge consumed by HER is considerably lower in cycle 452 as compared to cycle 5, with all the other cycles in between marking a transition from the initial to the final state of the iron electrode formation.

Examining the results for the hydrogen evolution shown in Figure 2b more closely, it can be seen that FE(HER) is the lowest for an electrode potential as high, or almost as high as the dip potential, while significantly less positive potentials cause more intense HER with a smooth transition from minimum to maximum HER in between. This observation corresponds to the previous deduction of a most intense $Fe(OH)_2$ reduction at an electrode potential as positive as the dip potential and a smooth transition to predominant HER beyond the dip. Moreover, it may also be observed that FE(HER) never drops to 0 % meaning that, regardless of the state of the iron electrode formation, for the present cycling procedure and iron electrode composition there will always be a certain minimum of charge that is diverted to HER. In addition, it is also interesting to see that the decrease in iron electrode potential beyond the dip coincides with the increase of FE(HER), eventually reaching FE(HER) = 100 %, if the progression of the iron electrode formation is low, i.e., if the currently available discharge capacity is clearly below the steady-state capacity (cycle < 325). And, conversely, if the currently available discharge capacity is close to the steady-state (cycle > 325), FE(HER) does not reach 100 % anymore, as the recharge period ends before exclusive HER.

From a battery perspective, the HER is an irreversible charge loss mechanism since the applied charge that is converted into hydrogen leaves the system in the form of gas bubbles and will not be available for the discharge reaction afterwards. Consequently, the extent of $Fe(OH)_2$ reduction is diminished by the charge lost due to HER, since the amount of applied charge per cycle is fixed to $Q_{chr} = 200\ mAh/g_{Fe}$ in the present study. Thus, from Avr.FE(HER), the total amount of charge that is lost by HER during the recharge ($Q_{HER\text{-}loss}$) can be calculated as [Eq. (4)]:

$$Q_{HER\text{-}loss} = \text{Avr.FE(HER)} \cdot Q_{chr} \quad (4)$$

Performing the corresponding calculation based on the results for FE(HER) shown in Figure 2b provides Figure 3, which identifies the HER as the only charge loss mechanism during the recharge of the investigated iron electrode. In fact, as it can be seen in Figure 3, Q_{dis} and $Q_{HER\text{-}loss}$ add up to $Q_{chr} = (200 \pm 2)\ mAh/g_{Fe}$, as the decrease of $Q_{HER\text{-}loss}$ mirrors the increase of Q_{dis} during the formation and continued electrochemical cycling in the steady-state. Consequently, the HER during the recharge has to be reduced in order to increase Q_{dis} according to Equation (5):

$$Q_{dis} = (1 - \text{Avr.FE(HER)}) \cdot Q_{chr} \quad (5)$$

Research Article
doi.org/10.1002/batt.202100415
Chemistry Europe
European Chemical Societies Publishing

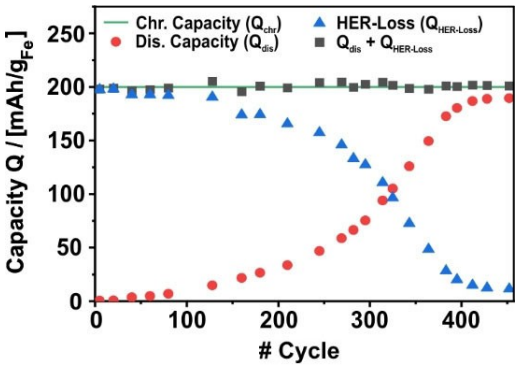

Figure 3. Progression of the discharge capacity (Q_{dis}) and the discharge capacity-loss due to the hydrogen evolution reaction (HER) as derived by Equation 4 ($Q_{HER-Loss}$) for the carbonyl iron electrode in Figure 1 and 2.

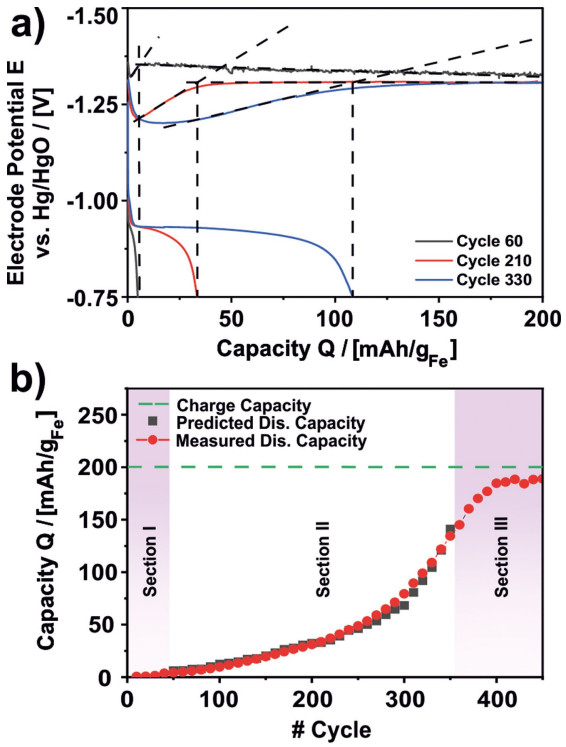

Figure 4. Derivation of the transition point-criterion to distinguish predominant $Fe(OH)_2$-reduction and HER based on characteristic charge potential profile features. a) The transition point is given by the abscissa for the intersection of two lines approximating the charge potential decrease beyond the potential dip and the potential plateau. The abscissa equals the discharge capacity of the subsequent discharge step (predicted dis. capacity) during the formation. b) Comparison for the actual and the predicted discharge capacity based on the transition point-criterion derived in a).

Mitigation of the HER

In the previous section, it has been described that the hydrogen evolution is a persistent reaction that appears during both the formation and continuous electrochemical cycling of a carbonyl iron electrode in alkaline electrolyte and should be reduced in order to increase the charging efficiency during the electrochemical cycling. In the following section, a total of three measures addressing this issue will be investigated and discussed.

Considering the individual course of the HER during the formation as shown in Figure 2b, it can be observed that a considerable amount of charge during the iron electrode reduction, prior to the steady state of the discharge capacity (see Figure 1b), is lost due to overcharging, indicated by FE(HER) = 100 %. Thus, in every recharge step, at least beyond the first moment in time when FE(HER) reaches 100 %, the electrochemical reduction of the iron electrode can be assumed to be neglectable and can, therefore, be avoided.

A possible indicator for the beginning of overcharging in terms of the electrode potential aside from the full observation of a potential plateau could be the transition point from the potential dip to the potential plateau, which could be used to mitigate the HER during the formation as shown in Figure 4a. In fact, the capacity applied until the intersection of two lines approximating the charge potential decrease beyond the potential dip on the one hand and the potential plateau on the other hand (predicted dis. capacity) coincides well with the discharge capacity of the subsequent discharge step, since the potential dip is associated with predominant $Fe(OH)_2$-reduction prior to hydrogen evolution,[23] while the potential plateau is associated with extensive HER. Thus, beyond the transition point, HER is most likely, but not necessarily 100 %, for a large number of formation cycles. Unfortunately, the transition point-criterion cannot be applied for the whole formation procedure. As indicated by Section I and III in Figure 4b, there are two periods during the formation, which prevent a consistent electrode potential dependent limitation of the recharge step. In Section I, a limitation of the recharge step by the transition point-criterion is prevented due to the missing potential dip, as shown by cycle 5 and 41 in Figure 2a, respectively. Moreover, in Section III, a limitation of the recharge step is prevented as well since a clear potential plateau is not observed in the charge curves beyond cycle 350 anymore. Nevertheless, in Section II, the transition point-criterion can be applied in order to mitigate the HER and to expedite the formation in terms of the elapsed time.

Considering the course of the HER during the continued electrochemical cycling in the steady-state (Figure 1c), here two possible measures to mitigate the HER are considered:

i. Application of a more negative cut-off potential during the discharge.
ii. Limitation of the electrode potential during the recharge.

Measure (i) results from the idea that an incomplete oxidation of the available active iron surface facilitates the subsequent reduction during the recharge, due to a thinner and/or non-continuous passivating $Fe(OH)_2$-layer.[35,42] Measure (ii) stems from the observation shown in Figure 5, which depicts the development of the electrode potential-dependent intensity of the HER, depending on the state of the iron electrode formation.

In Figure 5 it can be seen that the efficiency for the HER on the investigated iron electrode is not constant, but changes depending on the state of the iron electrode formation. In the beginning of the formation, e.g., after 80 cycles, predominant

Research Article
doi.org/10.1002/batt.202100415
Chemistry Europe
European Chemical Societies Publishing

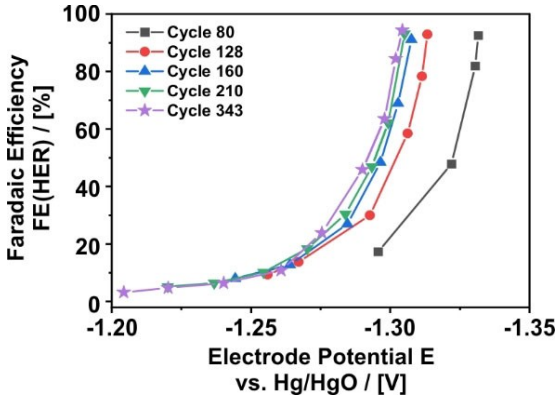

Figure 5. Development of the electrode potential-dependent intensity of the hydrogen evolution reaction (HER) as a result of the electrochemical formation of a pressed-plate carbonyl iron electrode in 6 M KOH at ambient temperature.

hydrogen evolution (i.e., FE(HER) > 50 %) is observed for comparatively low electrode potentials of about −1.32 V. However, due to the increasing surface area of the electrode during the formation, the onset of intense hydrogen evolution continuously increases to more positive potentials. Here, after 343 charge/discharge cycles, FE(HER) > 50 % is observed at an electrode potential of about −1.29 V, while FE(HER) > 10 % is observed at an electrode potential of −1.25 V. In addition, there is also very little change for the electrode potential-dependent intensity of the HER beyond cycle 160. Thus, especially in the steady-state, electrode potentials more negative than −1.25 V should be avoided, in order to increase CE(Q_{chr}). At this, it shall be noticed that a limitation of the electrode potential during the recharge requires a limitation of the applied charge current, which, in turn, extends the charging duration.

Confirming the previous suggestions with respect to measures (i) and (ii), Figure 6 and Table 1 provide the cycling procedures, the recorded charge/discharge patterns, the resulting change of the discharge capacity and exemplary HER-curves for corresponding cycling experiments. In Figures 6a–d, the influence of the altered charge/discharge patterns on the electrode potential can be seen. Comparing Figure 6a and b (see also Figure S4), it is clear that a more negative cut-off potential of −0.90 V as compared to −0.75 V lowers the potential overshoot in the beginning of the subsequent charge step, which slightly increases the resulting discharge capacity from 188.2 mAh/g_{Fe} (CE(Q_{chr}) = 94.1 %) to 189.6 mAh/g_{Fe} (CE-(Q_{chr}) = 94.8 %) as shown in Figure 6e and Table 1. At this, it can be seen in Figure 6e that the investigated electrode requires

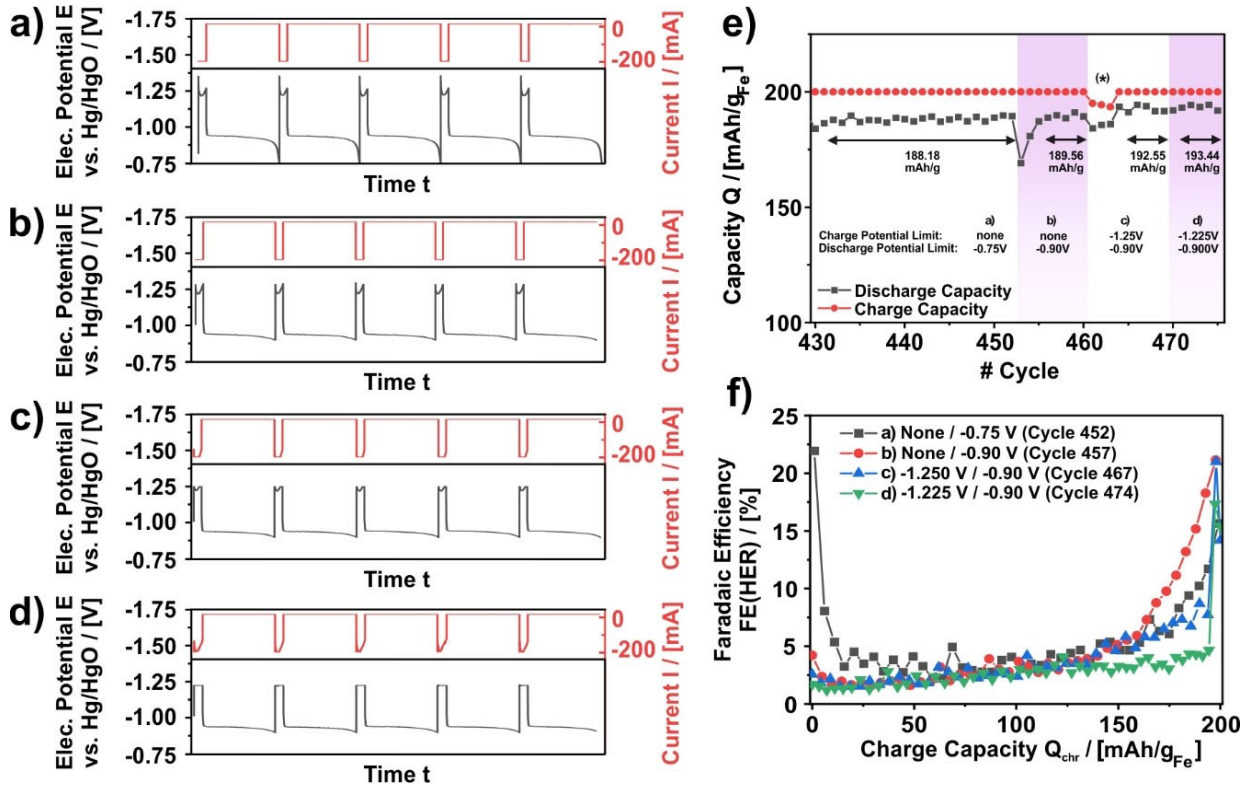

Figure 6. Impact of charge and discharge potential limitation on the discharge capacity and hydrogen evolution reaction (HER) during the electrochemical cycling of a formed carbonyl iron electrode in the steady-state of the discharge capacity (6 M KOH, ambient temperature). a–d) Charge/discharge potential profiles depending on the applied limitations. a) Standard cycling procedure: no charge potential limitation, −0.75 V discharge potential limitation. b) Altered cycling procedure: no charge potential limitation, −0.90 V discharge potential limitation. c) Altered cycling procedure: −1.25 V charge potential limitation, −0.90 V discharge potential limitation. d) Altered cycling procedure: −1.225 V charge potential limitation, −0.90 V discharge potential limitation. e) Charge and discharge capacity corresponding to the individual cycling procedures shown in a–d). ((*) indicates a transition period between b) and c) where the charging duration had falsely been limited to 1 h.) f) Exemplary course of the HER along with one charging step during the cycling procedure in a)–d) each.

Table 1. Overview over the results for the investigation of the impact of charge and discharge potential limitation on the discharge capacity and the extent of the HER in the steady-state of a carbonyl iron electrode in 6 M KOH at ambient temperature (Avr. FE(HER) = average Faradaic efficiency for the HER).

Cycling procedure	Cut-off potential (discharge) [V]	Charge potential limit [V]	Avr. discharge capacity [mAh/g_{Fe}]	Avr. charging efficiency [%]	Avr. FE(HER) [%]	Minimum FE(HER) [%]
a	−0.75	none	188.2*	94.1	5.9	2.2
b	−0.90	none	189.5	94.8	5.1	1.6
c	−0.90	−1.250	192.5	96.3	4.0	1.5
d	−0.90	−1.225	193.4	96.7	3.4	1.3

three cycles to attain a new steady-state after the cut-off potential was lowered. The latter results from the fact that the discharge stops earlier (= lower discharge capacity for the particular cycle) and disturbs the equilibrium between the gain in surface area during the electrochemical cycling and the loss of active surface area due to incomplete reduction, which is the explanation for the steady-state of the discharge capacity.[22] The increase in discharge capacity due to the more negative cut-off potential is a direct result of the lower hydrogen evolution in the beginning of the subsequent recharge step. Comparing the exemplary plots for the HER during the cycling procedures a) and b) in Figure 6f, it is particularly obvious that a more negative cut-off potential suppresses the HER in the beginning of the recharge step, lowering $Q_{HER\text{-}loss}$ enough to affect Q_{dis} positively. The lower intensity of the HER could be a result of a thinner or discontinuous passivating layer on the iron surface, which would arise from an incomplete discharge and might be reduced at a lower overpotential than a complete or thicker passivating layer that resulted from a complete discharge. Thus, −0.90 V is a more appropriate cut-off potential for the discharge reaction than −0.75 V upon the electrochemical cycling in the steady-state, since the more negative cut-off potential helps to increase the charging efficiency.

Furthermore, investigating the effect of a charge potential limitation, Figure 6c displays the influence for a limit of −1.25 V on the applied current and the electrode potential profile. From the comparison with Figures 6a–b it can be seen that the electrode potential is cut-off particularly at the end of the charging step, achieved by a lower charge current and resulting in a slightly longer charging period to maintain Q_{chr} = 200 mAh/g_{Fe}. As a result of the novel charging strategy, the average discharge capacity of the iron electrode in the steady-state increases from 189.6 mAh/g_{Fe} (CE(Q_{chr}) = 94.8 %) to 192.6 mAh/g_{Fe} (CE(Q_{chr}) = 96.3 %), which can be seen in Figure 6e. Similar to the impact of the cut-off potential, the increase of the discharge capacity is again a result of a mitigated HER as shown in Figure 6f. Comparing the exemplary HER-plots for cycling procedure b) and c), it can be seen that the HER for a limited charge potential of −1.25 V is particularly lowered at the end of the charging step as compared to the unlimited charge potential. At this, the mitigated HER coincides with a lower charge current during this period, which appears to be a more appropriate charge setting than a constant current of 200 mA/g_{Fe} for the whole charging period. In fact, a constant current/constant voltage step provides higher discharge capacities, while −1.25 V is not the optimum charge potential limit, yet. In Figure 6e it can be seen that a more positive charge potential limit of −1.225 V provides even higher discharge capacities of 193.4 mAh/g_{Fe} (CE(Q_{chr}) = 96.7 %). However, the gain in average discharge capacity (+0.8 mAh/g_{Fe}) is not as high as for the general introduction of a charge potential limitation (+3.0 mAh/g_{Fe}), which is mostly related to a very similar course of the HER as shown in Figure 6f. Particularly at the end of the charging step, the HER described by the exemplary plots for cycling procedure c) and d) jumps to significant values above FE(HER) = 15 %, which might be related to a complete reduction of $Fe(OH)_2$ resulting from the previous discharge step. Moreover, it is clear that Q_{dis} may not rise considerably anymore, as compared to cycling procedure c), since FE(HER) never drops to zero, regardless of the applied charge potential limit. In fact, the lowest momentary hydrogen evolution, FE(HER) = 1.29 %, is found for the charge settings shown in Figure 6d, while Avr.FE(HER) is as high as 3.4 % under these conditions (Table 1). Thus, a significant increase in charging efficiency can only be achieved in case the minimum intensity of the HER is decreased further. The latter can be achieved by an optimization of the electrode composition, e.g., Bi_2S_3 content, which shall be a focus for future research.

Conclusion

In the present study the hydrogen evolution reaction (HER) on pressed-plate carbonyl iron electrodes was investigated during the formation and electrochemical cycling in 6 M KOH using in situ gas chromatography. The investigation aimed to correlate the intensity of the HER and the applied electrode potential during the reduction of the iron electrodes. As a result, it was found that the HER follows a distinctive profile depending on the electrode potential and the state of the iron electrode formation. During the reduction of an iron electrode containing 8.5 wt.% Bi_2S_3, the intensity of the HER reached its individual minimum for the most positive electrode potential and typically varied between 2 % and 100 % in terms of momentary Faradaic efficiency (FE(HER)). However, the HER did not reach FE(HER) = 100 % in case the state of formation was advanced, i.e., in case the charge required to reduce the amount of accumulated $Fe(OH)_2$ on the iron electrode was close to the applied charge capacity per cycle. Under the applied cycling conditions, i.e., for immediate dis- after recharge, the decrease of the average HER-intensity per cycle mirrored the increase of the maximum discharge capacity, identifying the HER to be the only charge loss mechanism during the iron electrode reduction. Thus, the lower FE(HER),

the higher the discharge capacity for a preset charge capacity will be. Furthermore, it was found that the onset potential for intense hydrogen evolution changes depending on the state of the iron electrode formation, with the FE(HER) exceeding 10% at an electrode potential of −1.25 V at the end of the formation. Accordingly, the maximum discharge capacity could be increased by a limitation of the most negative charging potential, while a more negative cut-off potential during the discharge has a clearly beneficial influence on the iron electrode performance as well. In the present study, the highest charging efficiency for the repeated electrochemical cycling of a pressed-plate carbonyl iron electrode between −0.900 V and −1.225 V was 96.7% at a charge capacity of 200 mAh/g_{Fe}.

Experimental Section

Electrode preparation

Pressed-plate carbonyl iron electrodes were prepared from 1.0 g carbonyl iron powder (Sigma Aldrich, 3–5 μm, ≥99.5%, Germany), 100 mg (=8.5 wt.%) bismuth sulfide (Bi_2S_3, 99.9%, Alfa Aesar, Germany) and 70 mg polyethylene powder (PE, MW=4000 g/mol, Sigma Aldrich, Germany). For the preparation, the individual components were thoroughly mixed, heated to 140 °C and pressed to a pellet at a load of 88 MPa using an uniaxial die press (P/O/Weber, Germany). The resulting pellets had a diameter of 17 mm and a thickness of about 1.2 mm. The pellets were attached to a chemical resistant stainless steel rod as an electrode contact providing the investigated iron electrodes.

Electrochemical testing

For the electrochemical testing, a three electrode setup was applied, using the carbonyl iron electrodes as a working electrode, a platinum wire as a counter electrode and a Hg/HgO electrode (ALS, Japan) as a reference. 6 M KOH electrolyte was prepared from KOH pellets (EMSURE, Merck, Germany) using highly purified water (18.2 MΩ, Purelab, ELGA Veolia, United Kingdom). A VSP-300 (Bio-Logic, France) was used as a potentiostat, applying galvanostatic charge/discharge currents. As a standard setting for the electrochemical formation −200 mA were applied to the working electrode for 1 h, resulting into a charge capacity of Q_{chr}= 200 mAh/g_{Fe}. For the discharge, 20 mA were applied until a working electrode potential of −0.75 V was reached (cut-off potential). All electrode potentials in this paper are reported with respect to the Hg/HgO reference potential (+0.098 V vs. standard hydrogen electrode, SHE) unless stated otherwise.

HER monitoring

Aiming at a precise and prompt analysis of the hydrogen evolution reaction (HER) on the investigated iron electrodes, the three electrode setup was sealed and largely filled with electrolyte, minimizing the head space volume of the cell (Figure S1). The remaining head space volume was continuously purged with Argon (5.2 N, Air Liquid, France) at a flow rate of 144 mL/min. The gas outlet of the cell was connected to the inlet of a gas chromatograph at an inlet pressure of 50 mbar above ambient atmosphere. The gaseous reaction products were quantified on a Trace 1310 gas chromatograph (GC, Thermo Fischer, United States of America). The gas samples were injected from sample loops coupled directly to the experiment via a heated transfer line. H_2 was separated on 2 m×1 mm Haysep Q and 2 m×1 mm 5 Å molecular sieves packed columns coupled to a thermal conductivity detector (TCD). To minimize the analysis time, the pre-column was back-flushed after the retention time of H_2. The average run time for the GC was about 87.5 s, allowing 40–42 GC runs per hour. Calibration gas (Linde, GER) containing (1.67±0.02)% H_2 was used as a reference. The HER was discontinuously monitored along with the electrochemical cycling of the iron electrode. For an exemplary analysis of the resulting data (Figure S5), see Figure S2.

Acknowledgements

The authors kindly acknowledge the financial support from the German Federal Ministry of Education and Research within the project 'iNEW2.0 – Inkubator Nachhaltige Elektrochemische Wertschöpfungsketten' Project No. 03SF0627A and project 'FeE-nergy – Eisen-Slurry-Luft Akkumulator für die stationäre Energiespeicherung mit hoher Energiedichte' Project No. 13XP0188. Open Access funding enabled and organized by Projekt DEAL.

Conflict of Interest

The authors declare no conflict of interest.

Keywords: metal-air batteries · iron electrodes · hydrogen evolution reaction · in situ gas chromatography · quantitative analysis

[1] S. R. Sinsel, R. L. Riemke, V. H. Hoffmann, *Renewable Energy* **2020**, *145*, 2271–2285.
[2] P. Styring, E. A. Quadrelli, K. Armstrong, *Carbon Dioxide Utilisation*, Elsevier, Amsterdam, **2015**.
[3] S. R. Foit, R.-A. Eichel, I. C. Vinke, L. G. J. de Haart, *Angew. Chem. Int. Ed. Engl.* **2016**, DOI 10.1002/anie.201607552.
[4] B. R. de Vasconcelos, J. M. Lavoie, *Front. Chem.* **2019**, *7*, 1–24.
[5] R. Meys, A. Kätelhön, M. Bachmann, B. Winter, C. Zibunas, S. Suh, A. Bardow, *Science* **2021**, *374*, 71–76.
[6] S. Sripad, D. Krishnamurthy, V. Viswanathan, *ECSarXiv* **2021**, 1–17.
[7] H. Weinrich, Y. E. Durmus, H. Tempel, H. Kungl, R. A. Eichel, *Materials (Basel).* **2019**, *12*, DOI 10.3390/ma121321341–55.
[8] R. D. McKerracher, C. Ponce de León, R. G. A. Wills, A. A. Shah, F. C. Walsh, *ChemPlusChem* **2015**, *80*, 323–335.
[9] S. R. Narayanan, G. K. Surya Prakash, A. K. Manohar, B. Yang, S. Malkhandi, A. Kindler, *Solid State Ionics* **2012**, *216*, 105–109.
[10] S. S. Montiel Guerrero, Y. E. Durmus, K. Dzieciol, S. Basak, H. Tempel, S. Waasen, H. Kungl, R. Eichel, *Batteries & Supercaps* **2021**, *4*, 1830–1842.
[11] T. N. T. Tran, M. P. Clark, H. Chung, D. G. Ivey, *Batteries & Supercaps* **2020**, *3*, 409–416.
[12] Thomas A. Edison, *United States Patent Office*, **1905**, US797845.
[13] A. J. Salkind, C. J. Venuto, S. U. Falk, *J. Electrochem. Soc.* **1964**, *111*, 493–495.
[14] J. F. Jackovitz, G. A. Bayles, in *Handb. Batter.* (Eds.: D. Linden, T. B. Reddy), McGraw-Hill, New York, **2002**, pp. 720–746.
[15] L. Öjefors, L. Carlsson, *J. Power Sources* **1977**, *2*, 287–296.
[16] A. K. Manohar, S. Malkhandi, B. Yang, C. Yang, G. K. Surya Prakash, S. R. Narayanan, *J. Electrochem. Soc.* **2012**, *159*, A1209–A1214.
[17] A. K. Manohar, C. Yang, S. Malkhandi, B. Yang, G. K. Surya Prakash, S. R. Narayanan, *J. Electrochem. Soc.* **2012**, *159*, A2148–A2155.
[18] R. D. McKerracher, C. Alegre, V. Baglio, A. S. Aricò, C. Ponce De León, F. Mornaghini, M. Rodlert, F. C. Walsh, *Electrochim. Acta* **2015**, *174*, 508–515.

[19] H. A. Figueredo-Rodríguez, R. D. McKerracher, M. Insausti, A. G. Luis, C. Ponce De León, C. Alegre, V. Baglio, A. S. Aricò, F. C. Walsh, *J. Electrochem. Soc.* **2017**, *164*, A1148–A1157.
[20] A. K. Manohar, C. Yang, S. Malkhandi, G. K. S. Prakash, S. R. Narayanan, *J. Electrochem. Soc.* **2013**, *160*, A2078–A2084.
[21] H. A. Figueredo Rodriguez, R. D. Mckerracher, C. Ponce De León, F. C. Walsh, *J. Electrochem. Soc.* **2019**, *166*, A107–A117.
[22] H. Weinrich, M. Gehring, H. Tempel, H. Kungl, R.-A. Eichel, *J. Appl. Electrochem.* **2018**, *48*, 451–462.
[23] A. Sundar Rajan, M. K. Ravikumar, K. R. Priolkar, S. Sampath, A. K. Shukla, *Electrochem. Energy Technol.* **2014**, *1*, 2–9.
[24] K. Hayashi, Y. Wada, Y. Maeda, T. Suzuki, H. Sakamoto, W. K. Tan, G. Kawamura, H. Muto, A. Matsuda, *J. Electrochem. Soc.* **2017**, *164*, A2049–A2055.
[25] J. O. G. Posada, P. J. Hall, *J. Power Sources* **2014**, *262*, 263–269.
[26] A. R. Paulraj, Y. Kiros, B. Skårman, H. Vidarsson, *J. Electrochem. Soc.* **2017**, *164*, A1665–A1672.
[27] H. Wang, Y. Liang, M. Gong, Y. Li, W. Chang, T. Mefford, J. Zhou, J. Wang, T. Regier, F. Wei, H. Dai, *Nat. Commun.* **2012**, *3*, 917–918.
[28] B. T. Hang, D. H. Thang, E. Kobayashi, *J. Electroanal. Chem.* **2013**, *704*, 145–152.
[29] J.-S. Lee, S. T. Kim, R. Cao, N.-S. Choi, M. Liu, K. T. Lee, J. Cho, *Adv. Energy Mater.* **2011**, *1*, 34–50.
[30] Y. Li, H. Dai, *Chem. Soc. Rev.* **2014**, *43*, 5257–5275.
[31] J. Pan, X. L. Tian, S. Zaman, Z. Dong, H. Liu, H. S. Park, B. Y. Xia, *Batteries & Supercaps* **2019**, *2*, 336–347.
[32] Z. He, F. Xiong, S. Tan, X. Yao, C. Zhang, Q. An, *Mater. Today* **2021**, *11*, 1–13.
[33] C. Yang, A. K. Manohar, S. R. Narayanan, *J. Electrochem. Soc.* **2017**, *164*, A418–A429.
[34] A. Sundar Rajan, S. Sampath, A. K. Shukla, *Energy Environ. Sci.* **2014**, *7*, 1110–1116.
[35] H. Weinrich, J. Come, H. Tempel, H. Kungl, R.-A. Eichel, N. Balke, *Nano Energy* **2017**, *41*, 706–716.
[36] H. Weinrich, M. Gehring, H. Tempel, H. Kungl, R.-A. Eichel, *Electrochim. Acta* **2019**, *314*, 61–71.
[37] J. O. G. Posada, P. J. Hall, *Int. J. Hydrogen Energy* **2016**, *41*, 20807–20817.
[38] M. Chamoun, B. Skårman, H. Vidarsson, R. I. Smith, S. Hull, M. Lelis, D. Milcius, D. Noréus, *J. Electrochem. Soc.* **2017**, *164*, A1251–A1257.
[39] S. Malkhandi, B. Yang, A. K. Manohar, G. K. Surya Prakash, S. R. Narayanan, *J. Am. Chem. Soc.* **2013**, *135*, 347–353.
[40] H. Wu, C. Feng, L. Zhang, J. Zhang, D. P. Wilkinson, *Non-Noble Metal Electrocatalysts for the Hydrogen Evolution Reaction in Water Electrolysis*, Springer Singapore, **2021**.
[41] D. Mitra, A. S. Rajan, A. Irshad, S. R. Narayanan, *J. Electrochem. Soc.* **2021**, *168*, 030518.
[42] B. Tian, J. Światowska, V. Maurice, S. Zanna, A. Seyeux, P. Marcus, *Electrochim. Acta* **2018**, *259*, 196–203.
[43] F. M. Mulder, B. M. H. Weninger, J. Middelkoop, F. G. B. Ooms, H. Schreuders, *Energy Environ. Sci.* **2017**, *10*, 756–764.
[44] B. T. Hang, T. Watanabe, M. Egashira, I. Watanabe, S. Okada, J.-I. Yamaki, *Electrochem. Solid-State Lett.* **2005**, *8*, A476.
[45] J. O. G. Posada, P. J. Hall, *J. Power Sources* **2014**, *268*, 810–815.
[46] A. Engelbrecht, C. Uhlig, O. Stark, M. Hämmerle, G. Schmid, E. Magori, K. Wiesner-Fleischer, M. Fleischer, R. Moos, *J. Electrochem. Soc.* **2018**, *165*, J3059–J3068.

Manuscript received: November 26, 2021
Revised manuscript received: January 24, 2022
Accepted manuscript online: February 2, 2022
Version of record online: February 25, 2022